



HAL
open science

Single-image photogrammetry for deriving tree architectural traits in mature forest stands: a comparison with terrestrial laser scanning

Kamil Kędra, Ignacio Barbeito, Mathieu Dassot, Patrick Vallet, Anna Gazda

► To cite this version:

Kamil Kędra, Ignacio Barbeito, Mathieu Dassot, Patrick Vallet, Anna Gazda. Single-image photogrammetry for deriving tree architectural traits in mature forest stands: a comparison with terrestrial laser scanning. *Annals of Forest Science*, 2019, 76 (1), pp.1-13. 10.1007/s13595-018-0783-x . hal-02436352

HAL Id: hal-02436352

<https://hal.science/hal-02436352v1>

Submitted on 13 Jan 2020

HAL is a multi-disciplinary open access archive for the deposit and dissemination of scientific research documents, whether they are published or not. The documents may come from teaching and research institutions in France or abroad, or from public or private research centers.

L'archive ouverte pluridisciplinaire **HAL**, est destinée au dépôt et à la diffusion de documents scientifiques de niveau recherche, publiés ou non, émanant des établissements d'enseignement et de recherche français ou étrangers, des laboratoires publics ou privés.



Distributed under a Creative Commons Attribution 4.0 International License



Single-image photogrammetry for deriving tree architectural traits in mature forest stands: a comparison with terrestrial laser scanning

Kamil Kędra¹ · Ignacio Barbeito^{2,3} · Mathieu Dassot⁴ · Patrick Vallet^{5,6} · Anna Gazda¹

Received: 16 May 2018 / Accepted: 13 November 2018 / Published online: 7 January 2019
© The Author(s) 2019

Abstract

• **Key message** We compared two methods for detailed individual tree measurements: single image photogrammetry (SIP), a simplified, low-cost method, and the state-of-the-art terrestrial laser scanning (TLS). Our results provide evidence that SIP can be successfully applied to obtain accurate tree architectural traits in mature forests.

• **Context** Tree crown variables are necessary in forest modelling; however, they are time consuming to measure directly, and they are measured in many different ways. We compare two methods to obtain crown variables: laser-based and image-based. TLS is an advanced technology for three-dimensional data acquisition; SIP is a simplified, low-cost method.

• **Aims** To elucidate differences between the methods, and validate SIP accuracy and usefulness for forest research, we investigated if (1) SIP and TLS measurements are in agreement in terms of the most widely used tree characteristics; (2) differences between the SIP traits and their TLS counterparts are constant throughout tree density and species composition; (3) tree architectural traits obtained with SIP explain differences in laser-based crown projection area (CPA), under different forest densities and stand compositions; and (4) CPA modelled with SIP variables is more accurate than CPA obtained with stem diameter-based allometric models. We also examined the correspondence between local tree densities extracted from images and from field measurements.

• **Methods** We compared TLS and SIP in a temperate pure sessile oak and mixed with Scots pine stands, in the Orléans Forest, France. Standard major axis regression was used to establish relations between laser-based and image-based tree height and diameter at breast height. Four SIP-derived traits were compared between the levels of stand density and species composition with a *t* test, in terms of deviations and biases to their TLS counterparts. We created a set of linear and linear mixed models (LMMs) of CPA_{TLS} , with SIP variables. Both laser-based and image-based stem diameters were used to estimate CPA with the published allometric equations; the results were then compared with the best predictive LMM, in terms of similarity with CPA_{TLS} measurement. Local tree density extracted from images was compared with field measurements in terms of basic statistics and correlation.

Handling Editor: John M Lhotka

Contribution of the co-authors Conceptualization, K.K., I.B. and A.G.; methodology, K.K., I.B., M.D. and P.V.; software, K.K. and M.D.; formal analysis, K.K., P.V., and M.D.; investigation, K.K., I.B., and M.D.; resources, P.V., I.B., M.D., and K.K.; data curation, K.K., I.B., M.D., and P.V.; writing original draft preparation, K.K., I.B., M.D., P.V., and A.G.; funding acquisition, K.K., I.B., and A.G.

Electronic supplementary material The online version of this article (<https://doi.org/10.1007/s13595-018-0783-x>) contains supplementary material, which is available to authorized users.

✉ Kamil Kędra
k.kedra@ur.krakow.pl; k.w.kedra@gmail.com

¹ Department of Forest Biodiversity, University of Agriculture in Krakow, Al. 29 Listopada, Krakow 31-425, Poland

² AgroParisTech, INRA, Silva, Université de Lorraine, 54000 Nancy, France

³ Southern Swedish Forest Research Centre, Swedish University of Agricultural Sciences, Box 49, Alnarp 230 53, Sweden

⁴ EcoSustain, Environmental Engineering Office, Research and Development, 31 rue de Volmerange, 57330 Kanfen, France

⁵ Irstea, UR EFNO, Domaine des Barres, 45290 Nogent sur Vernisson, France

⁶ University Grenoble Alpes, Irstea, UR LESSEM, 38000 Grenoble, France

• **Results** Tree height and diameter at breast height were reliably represented by SIP (Pearson correlation coefficients $r = 0.92$ and 0.97 , respectively). SIP measurements were affected by the stand composition factor; tree height attained higher mean absolute deviation (1.09 m) in mixed stands, compared to TLS, than in pure stands (0.66 m); crown width was more negatively biased in mixed stands (-0.79 m), than in pure stands (-0.05 m); and diameter at breast height and crown asymmetry were found unaffected. Crown width and mean branch angle were key SIP explanatory variables to predict CPA_{TLS} . The model was approximately 2-fold more accurate than the CPA allometric estimations with both laser-based and image-based stem diameters. SIP-derived local tree density was similar to the field-measured density in terms of mean and standard deviation (9.6 (3.5) and 9.4 (3.6) trees per plot, respectively); the correlation between both density measures was significantly positive ($r = 0.76$).

• **Conclusion** SIP-derived variables, such as crown width, mean branch angle, branch thickness, and crown asymmetry, were useful to explain tree architectural differences under different densities and stand compositions and may be implemented in many forest research applications. SIP may also provide a coarse measure of local competition, in terms of number of neighbouring trees. Our study provides the first test in mature forest stands, for SIP compared with TLS.

Keywords Tree architecture · Branching system · Variable selection · Temperate pure and mixed forests · Remote sensing · Allometry

1 Introduction

Tree architectural traits provide detailed information on crown geometry, such as the position, shape (i.e. morphology), size and orientation of modules that constitute the branching system. In this paper, we follow the definition of tree architecture proposed by Barthélémy and Caraglio (2007) and simplified by Martin-Ducup et al. (2016) as “spatial arrangement of the different parts of a tree at a given time”. Knowledge of tree architectural traits is important for a number of reasons, e.g. (i) they quantify the architecture of an individual tree (Poorter et al. 2003, 2006); (ii) they are susceptible to the external factors and thus useful for predicting aboveground biomass (Forrester et al. 2017); (iii) they are very useful in estimating tree plasticity, i.e. the ability of spontaneous adaptation to the changing environmental conditions (Barbeito et al. 2014; Takahashi 1996; Van de Peer et al. 2017); and (iv) they can be used for estimating tree vigour and may be helpful in predicting growth of trees and forest stands (Lee et al. 2014; Rust and Roloff 2002).

However, tree architectural traits are difficult to measure in the field, especially for large trees and in dense stands. Therefore, they are sometimes inferred from basic tree metrics (such as stem diameter) with allometric models, built from samples of empirical data (e.g. Pretzsch et al. 2015). Existing methods to measure architectural traits may be grouped as destructive or non-destructive, direct or indirect, detailed or general, expensive or low cost, time-consuming or fast ones. The destructive techniques, though direct and most accurate, exclude the possibility of repeated measurements. Conversely, three types of non-destructive methods have been recently used, namely, sight-, image- (photogrammetric) and laser-based techniques. The sight-based methods are common praxis in forest inventories (Fleck et al. 2011) and include some

general tree measurements, like tree height (H), crown length (CL), crown radii (CR) and crown width (CW), which may be gained with the use of a measuring tape and a hypsometer. The other two methods rely on remote sensing and have been developed since the nineteenth and the twentieth centuries, for photogrammetry and LiDAR (light detection and ranging), respectively. Ground-based remote sensing methods enable the acquisition of more detailed tree characteristics, like branch length (BL), branch thickness (BT) and branch angle (BA). Terrestrial laser scanning (TLS) is the most accurate and a popular technology, among the laser-based methods, for describing individual tree architecture (Liang et al. 2016), while image-based methods vary from multiple-image methods (Phattaralerphong and Sinoquet 2005) to analysis of a single-image (Gazda and Kędra 2017) approaches. TLS systems have been thoroughly calibrated (Liang et al. 2016); however, comparisons between TLS and photogrammetric methods are scarce. In one of such few studies, Delagrangé and Rochon (2011) found that multiple-image photogrammetry, which produces a three-dimensional (3D) voxel-based model, was especially useful for yielding the two-dimensional (2D) architectural traits, while TLS was the predominant method for gaining the 3D traits, with both methods resulting in acceptably accurate measurements. Liang et al. (2016) also argued that the advantages of image-based methods include size, weight and price of the equipment. In turn, TLS is best in wood quality assessment and measurement accuracy, compared to multiple-images, mobile laser scanning and personal laser scanning methods (Liang et al. 2016). Thus, TLS and photogrammetry may be seen as contrasting, yet complementary techniques. Here, we focus on a comparison between TLS and the single-image photogrammetry (SIP) (Gazda and Kędra 2017), which has not yet been calibrated with a well-established method.

The model species here, sessile oak (*Quercus petraea* (Matt.) Liebl.), is a deciduous, long-lived, competitive and stress tolerant species, widely distributed in Europe, of high ecological, commercial and cultural importance (Eaton et al. 2016; Saenz-Romero et al. 2017). Mature trees are known to display complex and diverse architectural patterns, initially following the Rauh's architectural model (Oldeman 1990), which make their architectural inventory a challenging task. Moreover, we compared both methods in a temperate pure sessile oak and mixed with Scots pine (*Pinus sylvestris* L.) forests. Species mixing may have a significant effect on tree architecture: larger and longer crowns are expected in case of target trees growing in mixtures (Barbeito et al. 2017; Bayer et al. 2013), which add variability to our tests of TLS and SIP.

From TLS, we obtain a 3D object, which allows to measure many tree characteristics, such as horizontal crown projection area (CPA_{TLS}), providing information on factors such as space occupied by an individual tree, its radial growth potential, leaf biomass, carbon sequestration and competitive interactions within forest canopy (Fleck et al. 2011; Pretzsch et al. 2015). From SIP, we obtain a 2D vertical representation of a tree system, which may serve to derive such traits as BA, BL or BT; however, horizontal crown projection cannot be measured with SIP. The main objective of this study was to elucidate differences between the two methods and validate SIP accuracy and usefulness for forest research. We addressed the following working hypotheses:

1. SIP and TLS measurements are in agreement in terms of the most basic and widely used tree characteristics.
2. The differences between the SIP traits and their TLS counterparts are constant throughout the tree density and species composition levels of the study.
3. Tree architectural traits obtained with SIP explain differences in laser-based CPA, under different forest densities and stand compositions.
4. CPA modelled with SIP variables is more accurate than CPA obtained with stem diameter-based allometric models.

Additionally, we compared local tree density extracted from images with the same variable extracted from field measurements.

2 Materials and methods

2.1 Study area and tree sampling

The study was conducted in the Orléans National Forest, Central France (47° 49' N, 2° 29' E). The area has a temperate continental climate with an oceanic influence: mean annual temperature is 10.8 °C, and mean annual rainfall is 729 mm

(1981–2010 data from the SAFRAN and ISBA analytical platforms, Météo-France; Durand et al. 1993). The soil is qualified as a primary planosol (IUSS Working Group 2014). This type of soil is poor and acidic ($C < 1\%$, $C/N < 20$, $pH = 4.5$). The first horizon is loamy sand lying on a more or less impermeable clay horizon about 50 cm deep; this leads to temporarily waterlogged conditions in winter and spring. The terrain is predominantly flat.

We measured 54 oak trees within a network of plots established by the OPTMix experiment (for details, see optmix.irstea.fr): oak pine tree mixture (Korboulewsky et al. 2015). The plots represented six stands, differing in such factors as species composition and tree density (Table 1). Thirty trees were selected for mixed species composition (sessile oak mixed with Scots pine) and 24 trees for pure oak plots. The DBH of target trees ranged between 10 and 40 cm. Stand density, expressed by the relative density index (RDI), varied from low (dynamic management scenario, $RDI = 0.4$) to moderate (conservative management scenario, $RDI = 0.7$). The measured trees were between 60 and 80 years old.

2.2 Field measurements

In the leafless period (March) of 2016, 54 oak trees were captured by both methods: TLS and SIP (Fig. 1). The TLS team consisted of two people while SIP was conducted by a single person. TLS measurements followed Dassot et al. (2012), which included placement of reference spheres and taking several laser scans around each target tree (with a FARO Focus^{3D}X130 scanner), from four different positions, to limit occlusion, and ensure the proper representation of the whole branching system. In the case of SIP, fieldwork was performed according to Gazda and Kędra (2017). The method required one high-resolution digital image per tree; Sony DSC-HX20V camera was used. The distance from each image taken as well as camera tilt (image angle) were kept constant for every target tree (20 m and 15°, respectively), to ensure comparable accuracy within SIP method. The image azimuth (image direction) was established as a resultant of the following: (a) best possible visibility of whole target tree and (b) capturing the largest crown asymmetry and/or largest crown width (estimated by visually examining the target tree's crown from below).

2.3 Data extraction

The TLS- and SIP-derived variables are presented and defined in Table 2. In the TLS method, each target tree was manually extracted from the global point cloud using PolyWorks software (PolyWorks, InnovMetric software Inc.); DBH_{TLS} , H_{TLS} and CPA_{TLS} tree characteristics were extracted following Barbeito et al. (2017). In this study, we did not perform point cloud downsampling, to take advantage of the high (subcentimetre) accuracy of the TLS point cloud. The TLS

Table 1 Basic characteristics of forest stands and target trees used in this study. P: pure sessile oak stands, M: oak mixed with Scots pine

Stand no.	Stand code	No. of plots/target trees	Target tree mean DBH _{TLS} (cm)	Mean basal area (m ² /0.03 ha)	Stand composition
1	O214	12	21.98	0.62	P
2	O12	12	22.82	0.66	P
3	O598	12	25.65	0.72	M
4	O57	12	22.25	0.79	M
5	O255	3	31.10	1.03	M
6	O108	3	27.10	1.25	M

measurements used in this study were distances between specific points of the point clouds or metrics of convex polygons derived directly from the data points. We have not used any fitting approaches (except for DBH), which would be necessary to obtain more advanced TLS traits, such as branch lengths and angles. Disentangling the errors of laser measurement and additional model fitting would overwhelm the main objectives of this study. CW_{TLS} and crown asymmetry (CWA_{TLS}) were extracted in QGIS software (QGIS Development Team 2016), from the vertices of crown projection polygons, their centroids and stem base centre points. Image vectorization of the SIP method followed Gazda and Kędra (2017). The five TLS-based traits under study relate differently to SIP-based traits: tree height was similarly defined in case of both methods, as the vertical distance between the lowest and highest parts of a tree; DBH, in TLS, was

assessed from least square circle fitting on a 2-cm-thick slice of points at 1.30 m height, and in SIP, it was measured within a selected plane (perpendicular to the image direction). Both traits, when measured with TLS, may attain some error, such as 0.5 m for tree height and 2 cm for DBH (Calders et al. 2015). TLS horizontal crown projection area was calculated from a convex crown polygon (see Barbeito et al. 2017) for a detailed explanation of the differentiation between a convex and non-convex crown polygon), and this trait could not be measured with SIP. TLS is a very accurate method to measure crown projection area (Fleck et al. 2011) and thus may be used as reference data. CW_{TLS} and CWA_{TLS} were also obtained in relation to the horizontal crown projection polygon, while crown width assessed with SIP (CW_{SIP}) and CWA_{SIP} related to the vertical crown polygon, measured in the selected plane (see Sect. 2.2 for details). For this reason, CW and CWA were

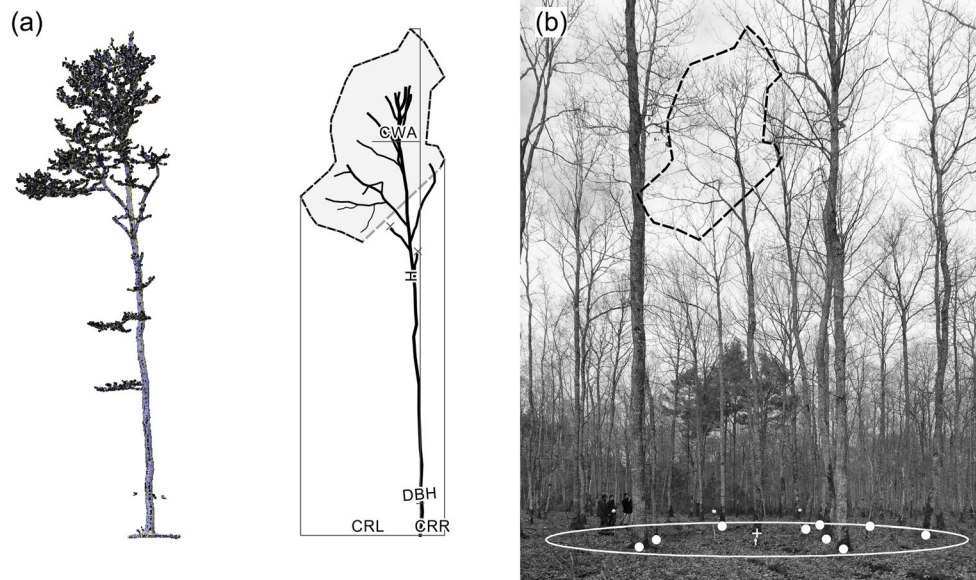


Fig. 1 **a** Comparison of two silhouettes from the same sessile oak tree. Left, TLS point cloud; right, digitized architecture obtained with the single image photogrammetric (SIP) method (software used: QGIS (QGIS Development Team 2016)); different line weights represent different orders of branches; basic measurements are shown: CRL (left crown radius), CRR (right crown radius), DBH (diameter at breast height), H

(tree height) and CWA (crown width asymmetry). The scale is constant for both silhouettes, the object size (height) measured with TLS is 20.75 m and 20.83 m measured with the image-based method. **b** Transformed image and measurement of number of trees neighbouring the target individual within an 8-m radius

Table 2 Description of the architectural traits measured with TLS or SIP methods

Method	Abbreviation	Mean (SD)	Unit	Description
TLS	H_{TLS}	18.44 (2.45)	m	Tree height, assessed as the vertical distance between the highest and the lowest point
	DBH_{TLS}	23.84 (6.21)	cm	Diameter at breast height, assessed from least square circle fitting on a 2-cm-thick slice of points at 1.30 m height
	CPA_{TLS}	36.04 (18.23)	m ²	Convex, horizontal crown projection area
	CWA_{TLS}	1.34 (0.76)	m	Crown width asymmetry; the horizontal distance between the horizontal crown projection centroid and stem base point
	CW_{TLS}	6.89 (2.01)	m	Crown width; crown projection polygon extent, along the direction of CWA_{TLS}
SIP	H_{SIP}	18.84 (2.82)	m	Tree height
	DBH_{SIP}	25.52 (6.45)	cm	Diameter at breast height, measured within a selected plane (perpendicular to the image direction)
	CA_{SIP}	49.88 (25.41)	m ²	Non-convex, vertical crown projection area
	CL_{SIP}	12.59 (3.81)	m	Crown length, assessed as the vertical distance between the highest and the lowest point of digitized live-crown envelope
	CW_{SIP}	6.42 (2.38)	m	Crown width ($CR_{\text{SIP}L} + CR_{\text{SIP}R}$), where $CR_{\text{SIP}L}$ and $CR_{\text{SIP}R}$ are two crown radii observed in the image (on the left and right sides of the stem, respectively)
	CWA_{SIP}	1.08 (0.74)	m	Crown width asymmetry ($CR_{\text{SIP}max} - CW_{\text{SIP}}/2$), where $CR_{\text{SIP}max}$ is $CR_{\text{SIP}L}$ or $CR_{\text{SIP}R}$, whichever greater
	AL_{SIP}	49.81 (21.81)	m	Total length of stem and branches
	MBL_{SIP}	2.06 (0.69)	m	Mean (per tree) 2nd-order branch length
	MBA_{SIP}	45.94 (13.31)	°	Mean (per tree) branch angle
	MBT_{SIP}	5.24 (1.82)	cm	Mean (per tree) 2nd-order branch thickness
FBH_{SIP}	8.73 (2.21)	m	Height of insertion of the first (lowest) branch	

excluded from direct comparison between SIP and TLS, which however, were included in the sensitivity analysis of SIP measurements in relation to stand conditions (Sect. 2.4.2). Three out of the five TLS-based traits are difficult to measure with common methods and are rarely available, namely CPA, CW and CWA.

In SIP, mean branch angle (MBA_{SIP}) was obtained as a mean value for optimally five particular branch angles (Fig. 2) within a single branching system. The set of individual branch angles consisted of largest angles between the main tree axis and the second order axes, distributed along crown length. We also kept that measurement when less than five second-order branches fulfilled the requirements. In the SIP, most precise measurements refer to those parts of a tree that are included within the measurement (projection) plane (Gazda and Kędra 2017); we assumed that largest branch angles belong to branches closest to the plane. The extraction of tree axes (skeletonization) preceded any other measurements; branches that underwent this procedure were not less than 2 cm thick; and the pixel size of transformed images was 6×6 mm. The angle measurement was similar to that presented in Bayer et al. (2013); however, in that study, the branch angle was instead related to the vertical direction. A single-tree data extraction, for all 11 SIP traits, took approximately 3 h on average, including some double-checking and breaks.

While in TLS, the single-tree data extraction (including tree separation) took approximately 1.5 h on average, for DBH, CPA vertices, tree base points and tree height.

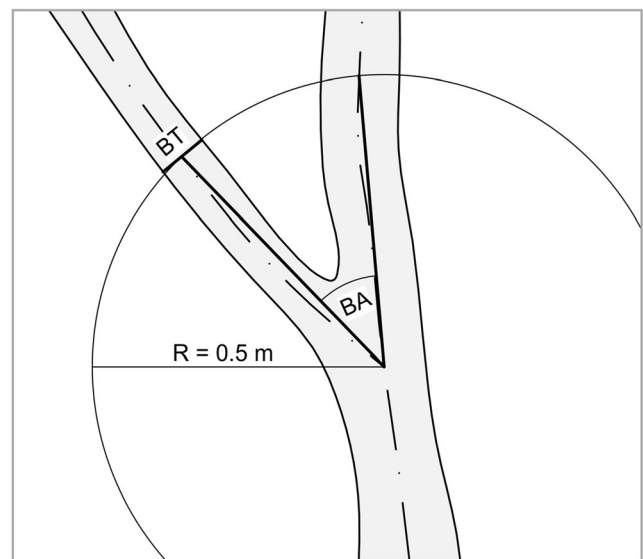


Fig. 2 Visual representation of a particular branch angle (BA_{SIP}) measurement with SIP method; BT is the thickness of the branch measured at the distance of 0.5 m from the branch insertion point; the software used for measurements was QGIS v.2.8.7 (QGIS Development Team 2016)

2.4 Data processing and statistical analyses

2.4.1 Tree height and diameter at breast height

For the two pairs of traits measured with TLS and SIP, which could be directly compared (tree heights: $H_{\text{TLS}}-H_{\text{SIP}}$ and diameters at breast height: $\text{DBH}_{\text{TLS}}-\text{DBH}_{\text{SIP}}$), we built standard major axis regression (SMA) models. We aimed at establishing relatedness between the traits coming from different methods in terms of Pearson product-moment correlation r , R -square and model slope values. SMA regression was more suitable here than a simple linear regression, because it can deal with variability (i.e. measurement errors) in both response and explanatory variables. All analyses were conducted in R v.3.4.1 statistical software (R Core Team 2017); the SMA models were fitted using the “lmodel2” package (Legendre 2014). We tested for multivariate normality in data with the “mvnTest” package (Anderson–Darling test) (Pya et al. 2016).

2.4.2 Sensitivity of SIP measurements to varying stand density and tree species composition

We assumed that the quality of TLS measurement was always very high, disregarding the stand variation of this study (Table 1). Thus, we could test if the deviations of SIP in relation to TLS differ significantly between contrasted stand conditions. To do that, two stand factor variables were used representing stand density and species composition. For stand density (in terms of the number of neighbouring trees, in the distance of up to 8 m from the target tree), there were two levels: lower density (between two and eight stems, with 29 observations) and higher density (between 9 and 19 stems, with 25 observations). For stand composition, there were also two levels: pure oak plots (24 observations) and oak mixed with pine (30 observations). Welch two-sample t test was used, as the sample sizes were unequal, with possibly different variances. The investigation included four variables: DBH, H, CW and CWA. We tested for non-zero differences in mean: absolute deviations (MAD), absolute percentage deviations (MAPD) and biases (SIP minus TLS measurements), between the levels of the two stand factors. Additionally, Pearson’s correlations between SIP measurements and their TLS counterparts were calculated to give the traits’ relatedness context.

2.4.3 Horizontal crown projection area

CPA_{TLS} had no such a direct counterpart in the SIP-derived trait set. Thus, we tested if such TLS-based variable could be modelled with a set of SIP variables. To select the best subset of SIP traits for further TLS trait modelling, we used the R package “olsrr” (Hebbali 2017), a tool for building and comparing ordinary least square (OLS) regression models. A total

number of 2047 OLS models were analysed. This included all possible combinations of the 11 SIP variables. Eleven subsets, including 1 to 11 predictors, were selected in terms of widely used model evaluation criteria: R -square, adjusted R -square, Mallow’s C_p and Akaike Information Criterion (AIC). Those were extracted from a longer list of criteria available with the R package (Hebbali 2017). Selected subsets of variables were then used to create linear mixed models (LMMs) with the “lme4” R package (Bates et al. 2015). All random effects were induced by forest stand (Table 1), to account for hierarchy (or nesting) of the data. We assumed that trees from a given stand were likely more similar to each other than trees from different stands, due to factors such as local soil composition and microclimate. The two stands, from which there were only three observations (O255, O108), were pooled together; they were similar in terms of tree density, target tree size and species composition. We propose a general modelling framework, as exemplified by subsets of up to three explanatory variables (Table 3).

Models indexed with the letter “a” allowed for random intercept only; all other LMMs allowed both random slopes and random intercepts, but the random effects, coming from five levels of stand, were connected to different variables within model groups, i.e. LMM[2b,c] and LMM[3b–d]. We compared the root mean squared errors (RMSE) of all LMMs and simple linear models (including the same variables), to test if adding another explanatory variable and including random effects made any difference in model performance. In all cases, RMSE values were obtained with model fitted values (RMSE1) and using a leave-one-out model analysis (RMSE2). Subsequently, the best predictive model was selected.

To test the fourth hypothesis, we used simple allometric models (Pretzsch et al. 2015), to predict crown radius ($\text{CR} = \text{half the crown diameter}$), with both DBH_{SIP} and DBH_{TLS} . The allometric models presented by Pretzsch et al. (2015) aim at predicting maximal crown dimension for a given stem diameter, are robust, created from large data sets (mainly from the Southern German long-term forest research plots) and include equations for 22 tree species and general models for 5 crown expansion types (groups of several species). Sessile oak was not among those 22 species, and therefore, we used the equation for the most closely related species from the list, pedunculate oak (*Quercus robur* L.):

$$\text{CR} = \exp(-1.4370) \times \text{DBH}^{0.8157}, \quad (1)$$

and the equation for sessile oak crown extension type (the same as for pedunculate oak):

$$\text{CR} = \exp(-1.4936) \times \text{DBH}^{0.7985}. \quad (2)$$

The crown dimensions were then used to estimate CPA ($\text{CPA} = \pi \times \text{CR}^2$). We compared both models with the best

Table 3 Summary of the modelling framework for building linear mixed models (LMMs) in this study; Trait_{xTLS} is the TLS-derived response variable (here CPA_{TLS}); Trait_{xnSIP} are the explanatory SIP-derived variables

No. of variables	Model ID	Formula ¹
1	LMM[1a]	trait _{xTLS} ~ trait _{x1SIP} + (1 stand)
	LMM[1b]	trait _{xTLS} ~ 1 + (trait _{x1SIP} stand)
2	LMM[2a]	trait _{xTLS} ~ trait _{x1SIP} + trait _{x2SIP} + (1 stand)
	LMM[2b]	trait _{xTLS} ~ (trait _{x1SIP} stand) + trait _{x2SIP}
	LMM[2c]	trait _{xTLS} ~ trait _{x1SIP} + (trait _{x2SIP} stand)
3	LMM[3a]	trait _{xTLS} ~ trait _{x1SIP} + trait _{x2SIP} + trait _{x3SIP} + (1 stand)
	LMM[3b]	trait _{xTLS} ~ (trait _{x1SIP} stand) + trait _{x2SIP} + trait _{x3SIP}
	LMM[3c]	trait _{xTLS} ~ trait _{x1SIP} + (trait _{x2SIP} stand) + trait _{x3SIP}
	LMM[3d]	trait _{xTLS} ~ trait _{x1SIP} + trait _{x2SIP} + (trait _{x3SIP} stand)

¹ R notation was used; the models accounted for unexplained deviance by either fixed or random (stand) effects, assumed to be normally distributed, with mean equal to zero

predictive model of this study (LMM or LM), in terms of similarity with CPA_{TLS}, by calculating RMSE and percentage RMSE.

2.4.4 Tree density obtained with SIP or field measurements

Gazda and Kędra (2017) highlighted the possibility to estimate tree density with SIP method. However, in that study, upland landscape strongly limited the use of that concept. Here, we estimated number of all mature trees (N_{SIP}) within a circular area of 8 m radius from each target tree (Fig. 1b). We compared those results with field measurements. Circles were fitted to the images with the use of a camera model in ArchiCAD software (<https://myarchicad.com/>). However, the circle may be also fitted with the use of a reference image, which is more widely accessible method to SIP users (Gazda and Kędra 2017). We assumed that the terrain was completely flat, and thus, the perspective image of the bounding circle (i.e. an ellipse) was always the same. Trees that were visually assessed as growing inside the circle were marked with a point in QGIS v.2.8.9 software (QGIS Development Team 2016). The outcome was a simple count of individuals. We compared this result to field measurements in terms of basic statistics (mean and standard deviation), Pearson correlation coefficient, and with a LMM, which allowed for a random intercept induced by stand differences.

3 Results

3.1 Tree height and diameter at breast height

For both pairs of variables (H_{TLS}–H_{SIP} and DBH_{TLS}–DBH_{SIP}), the distribution was bivariate normal; error variance on each axis was proportional to variance of corresponding variable; and correlation r was significant (Table 4). For both models (H_{TLS}~H_{SIP} and DBH_{TLS}~DBH_{SIP}), the correlation

coefficients were very high ($r > 0.9$). DBH measurement attained higher values in case of SIP compared with TLS within the whole range of measurements. While the H_{SIP} values were lower, compared with H_{TLS}, in case of smaller trees, and higher for higher trees, tree heights ranging ca. 15–17 m were estimated most similarly by both methods (Fig. 3).

3.2 Sensitivity of SIP measurements to varying stand density and tree species composition

In the studied range of stand variation, the SIP measurements were only affected significantly by the stand composition factor (Table 5). Interestingly, from the set of four traits derived from SIP (DBH_{SIP}, H_{SIP}, CW_{SIP} and CWA_{SIP}), tree height occurred to be the most sensitive one, being the most accurate at the same time. Both mean absolute deviation (MAD) and mean absolute percentage deviation (MAPD) were higher in mixed oak pine stands, compared to pure oak stands (by 0.43 m and 2.42%, respectively). However, we found no significant difference in bias of the measurements (0.24 m (1.29%) and 0.53 m (2.86%) for pure and mixed stands, respectively). In turn, CW_{SIP} was significantly more biased in mixed stands (–0.79 m (–10.30%)) versus pure stands (–0.05 m (–0.89%)), but there were no significant differences in MAD or MAPD, which were around 1 m or 16%, respectively. The other traits did not show significant variations in accuracy or precision. Nonetheless, the difference in MAD of CW_{SIP} was close to the 0.05 significance threshold (0.86 m in pure and 1.29 m in mixed stands; $p = 0.052$). DBH_{SIP} was the only trait seemingly affected by the stand density factor, in terms of MAPD (6.73% at lower density and 10.12% at higher density; $p = 0.057$). Crown width asymmetry appeared to be the most stable trait between the levels of both factors (MAD between 0.38 and 0.43 m; bias between –0.30 and –0.19 m). The lowest correlation with TLS measurement was for CW_{SIP} at higher density ($r = 0.77$) and the highest for DBH_{SIP} in mixed stands ($r = 0.98$); all correlations were significant ($p < 0.001$).

Table 4 Results for the Anderson–Darling test for multivariate normality (AD and p value) and SMA regression outputs for tree height ($H_{\text{TLS}} \sim H_{\text{SIP}}$) and diameter at breast height ($\text{DBH}_{\text{TLS}} \sim \text{DBH}_{\text{SIP}}$)

Model	AD	p value	r	SMA_slope	SMA_intercept
$H_{\text{TLS}} \sim H_{\text{SIP}}$	0.34	0.76	0.92	0.87 (40.92°)	2.11
$\text{DBH}_{\text{TLS}} \sim \text{DBH}_{\text{SIP}}$	0.94	0.14	0.97	0.96 (43.88°)	-0.70

measurements: Pearson product–moment correlation (r) and regression parameters (slope and intercept values)

3.3 Horizontal crown projection area

When setting CPA_{TLS} as the response variable and all the SIP-derived traits as potential explanatory variables, we obtained a list of possible subsets, ordered by the number of included variables (1 to 11) (Fig. 4). Table 6 presents membership of the best subsets and values for the criteria of selection. We decided to stop our analysis at the third subset ($\text{CW}_{\text{SIP}} + \text{MBA}_{\text{SIP}} + \text{MBT}_{\text{SIP}}$), because we observed little gain in AIC or Mallows' Cp when considering four or more explanatory variables.

On a second step, we created LMMs according to the formulas: LMM[1a] to LMM[3d] and the reference linear models (LMs) to predict TLS-derived horizontal crown projection area (CPA_{TLS}). The trends for both RMSE values were similar but always higher in case of the leave-one-out method (RMSE2) and differed by 0.32 to 2.14 m^2 (Table 7). Stand random effect on intercept only appeared to be effective in the first subset, with just CW_{SIP} as explanatory variable (LMM[1a]). Model LMM[2c] showed the best predictive performance (RMSE1 = 5.67; RMSE2 = 7.45 m^2); the model included random intercept and random slope for mean branch angle (MBA_{SIP}), as a result of differences in stand characteristics. This result improved the corresponding simple linear model, by 3.32 and 2.11 m^2 in terms of RMSE1 and RMSE2, respectively. For all subsets of explanatory variables, both RMSE1 and RMSE2 values were always lower in case of LMMs, compared with their reference LMs. The second best model (LMM[3c]) included three explanatory variables,

including MBT_{SIP} . In this model, the random effect was also combined with MBA_{SIP} , similarly as in the case of LMM[2c].

Crown projection area estimates with allometric Eq. (1) resulted on slightly higher RMSE from DBH_{SIP} (14.34 m^2) than from DBH_{TLS} (13.83 m^2), which correspond to percentage RMSE of 39.79 and 38.38%, respectively. The CPA predictions with Eq. (2) appeared slightly better in case of DBH_{SIP} (RMSE = 15.82 m^2 , percentage RMSE = 43.89%) than from DBH_{TLS} (RMSE = 16.85 m^2 , percentage RMSE = 46.75%). All the allometric CPA estimations were approximately 2-fold less accurate than that of model LMM[2c] and were rather negatively biased, compared to TLS reference measurement (e.g. -3.64 m^2 , for Eq. (1) with DBH_{TLS}).

3.4 Tree density obtained with SIP or field measurements

The LMM revealed a tendency to overestimation of number of trees by SIP at higher densities and underestimation at lower densities (model slope = 33.45°; Fig. 5). The model allowed a random intercept from five levels of stand; this led to a slight stratification in the model. Two stands resulted in visible displacements in the regression lines: O214 (highest intercept) and O598 (lowest intercept). The other three lines were much closer together. The Pearson's correlation for SIP and field data was significantly positive (Table 8).

Fig. 3 Relatedness of the TLS- and SIP-derived variables. Left, tree height (in metres); right, diameter at breast height (in centimetres); black solid lines are the SMA regression lines, grey lines represent 95% confidence intervals and dashed lines are the 45-degree lines

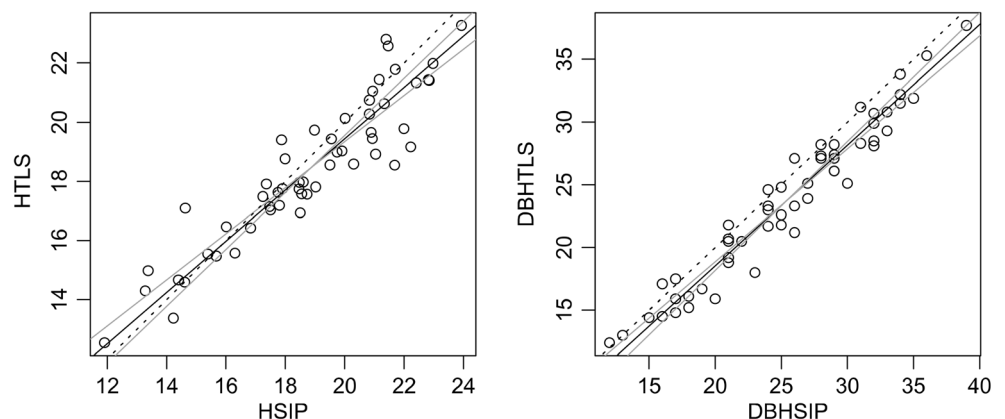


Table 5 Correlations, mean absolute deviations (MAD), mean absolute percentage deviations (MAPD) and biases of selected SIP measurement in relation to TLS measurements and between two stand factors: (a) stand density and (b) species composition; the statistical tests refer to Welch *t* test for differences in means; and significant differences at the 0.05 and 0.1 levels were denoted by bold font and by italics, respectively

Trait	Factor level	Correlation		Deviation		MAD <i>t</i> test			MAPD <i>t</i> test			Bias		Bias <i>t</i> test		
		r	<i>p</i> value	MAD ¹	MAPD ²	<i>t</i>	<i>df</i>	<i>p</i> value	<i>t</i>	<i>df</i>	<i>p</i> value	Bias ³	Bias %	<i>t</i>	<i>df</i>	<i>p</i> value
(a) Stand density																
DBH (cm)	Lower	0.969	2.2E-16	1.66	6.73	1.219	50.12	0.228	1.953	42.63	0.057	1.46	5.70	1.130	50.24	0.264
	Higher	0.971	7.17E-16	2.10	10.12							1.94	8.90			
H (m)	Lower	0.896	4.79E-11	1.03	5.56	-1.410	51.16	0.165	-1.363	50.99	0.179	0.39	2.09	0.029	50.25	0.977
	Higher	0.950	3.74E-13	0.76	4.14							0.40	2.24			
CW (m)	Lower	0.839	1.35E-08	1.06	14.34	0.318	43.95	0.752	1.331	38.05	0.191	-0.27	-3.56	-1.174	49.98	0.246
	Higher	0.767	7.67E-09	1.14	18.98							-0.69	-11.24			
CWA (m)	Lower	0.863	1.76E-09	0.39	38.53	0.382	35.86	0.705	0.402	51.28	0.690	-0.23	-17.08	-0.331	42.62	0.742
	Higher	0.783	3.78E-06	0.43	42.94							-0.28	-21.48			
(b) Species composition																
DBH (cm)	Pure	0.964	4.25E-14	2.10	9.84	-1.163	47.01	0.251	-1.561	41.55	0.126	1.93	8.61	-1.051	47.37	0.299
	Mixed	0.976	<2.2E-16	1.68	7.07							1.48	5.94			
H (m)	Pure	0.949	1.61E-12	0.66	3.56	2.344	50.75	0.023	2.461	49.99	0.017	0.24	1.29	1.005	50.35	0.320
	Mixed	0.928	1.64E-13	1.09	5.98							0.53	2.86			
CW (m)	Pure	0.894	4.11E-09	0.86	15.43	1.988	51.81	0.052	0.548	46.62	0.587	-0.05	-0.89	-2.183	51.99	0.034
	Mixed	0.816	3.99E-08	1.29	17.33							-0.79	-10.30			
CWA (m)	Pure	0.792	3.97E-06	0.38	42.37	0.368	45.41	0.715	-0.295	50.75	0.769	-0.19	-15.64	-0.849	45.61	0.401
	Mixed	0.809	6.25E-08	0.42	39.13							-0.30	-21.41			

¹ MAD = mean(abs(trait_{SIP} - trait_{TLS}))
² MAPD = mean(abs((trait_{SIP} - trait_{TLS})/trait_{TLS}))×100
³ Bias = mean(trait_{SIP} - trait_{TLS})

4 Discussion

4.1 Agreement between SIP and TLS

Our results showed that the SIP-derived global tree traits are in agreement with those obtained from TLS-based measurements. From the set of all analysed variables, only one aimed at measuring exactly the same quantity in case of both

methods, namely tree height (H_{SIP} or H_{TLS}). This trait was preliminarily assessed as the most influenced by the overall crown shape and branching pattern when measured with SIP: in case of trees with wide crowns and a sympodial growth, the error of H_{SIP} may be as high as 60%, because of crown self-occlusion; however, for species with monopodial growth, the error may be lower than 1% (Gazda and Kędra 2017). We cannot define the overall branching patterns of measured

Fig. 4 Graphical representations for the output of “ols_best_subset” function (package “olsr” in R); 11 subsets were distinguished, ranked by the number of included variables and criteria of model selection: *R*-square, adjusted *R*-square, Mallow’s *C*(*p*) and Akaike Information Criterion (AIC); grey horizontal and vertical lines denote subsets which improved the criteria

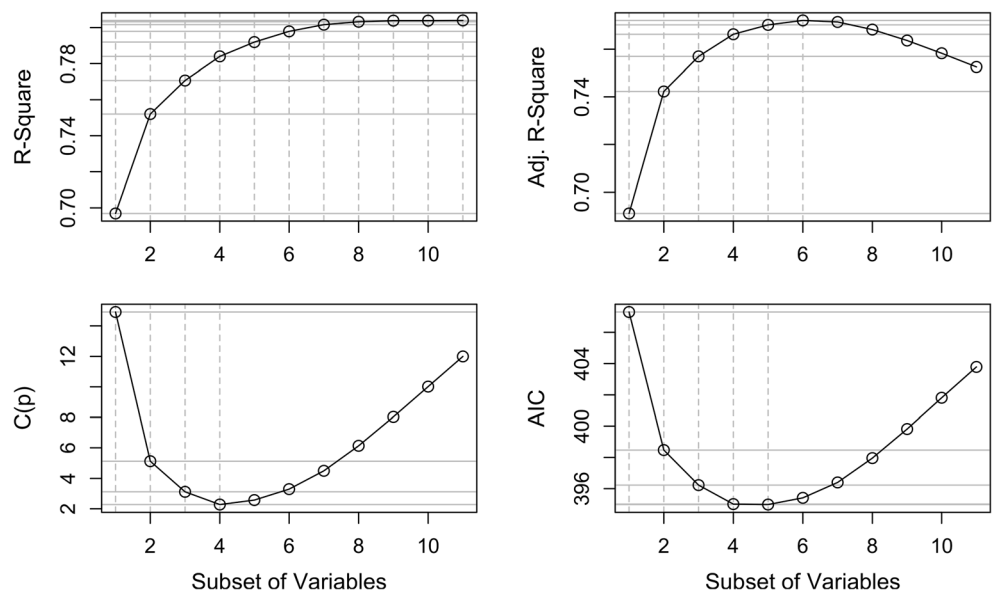


Table 6 Best subsets of SIP-derived variables to predict CPA_{TLS} ranked by the number of included variables (index) and criteria of model selection: R-square, adjusted R-square, Mallows’s C(p) and Akaike Information Criterion (AIC); three best subsets, analysed further, are denoted in italics

Index	Predictors	R-square	Adj. R-square	C(p)	AIC
1 (LM[1])	CW _{SIP} ***	0.70	0.69	14.92	407.30
2 (LM[2])	CW _{SIP} ***, MBA _{SIP} **	0.75	0.74	5.12	398.47
3 (LM[3])	CW _{SIP} ***, MBA _{SIP} ***, MBT _{SIP} *	0.77	0.76	3.12	396.24
4	CW _{SIP} ***, MBA _{SIP} ***, MBT _{SIP} [^] , CWA _{SIP} [^]	0.78	0.77	2.28	395.02
5	CW _{SIP} ***, MBA _{SIP} ***, MBT _{SIP} [^] , CWA _{SIP} [^] , FBH _{SIP}	0.79	0.77	2.56	394.99
6	CW _{SIP} ***, MBA _{SIP} ***, MBT _{SIP} , CWA _{SIP} [^] , H _{SIP} [^] , DBH _{SIP}	0.80	0.77	3.29	395.42
7	CW _{SIP} ***, MBA _{SIP} ***, MBT _{SIP} , CWA _{SIP} [*] , FBH _{SIP} , H _{SIP} , DBH _{SIP}	0.80	0.77	4.49	396.41
8	CW _{SIP} ** [*] , MBA _{SIP} ** [*] , MBT _{SIP} , CWA _{SIP} [*] , FBH _{SIP} , H _{SIP} , DBH _{SIP} , MBL _{SIP}	0.80	0.77	6.14	397.97
9	CW _{SIP} [^] , MBA _{SIP} ** [*] , MBT _{SIP} , CWA _{SIP} [*] , FBH _{SIP} , H _{SIP} , DBH _{SIP} , MBL _{SIP} , CA _{SIP}	0.80	0.76	8.03	399.82
10	CW _{SIP} , MBA _{SIP} [*] , MBT _{SIP} , CWA _{SIP} [^] , FBH _{SIP} , H _{SIP} , DBH _{SIP} , MBL _{SIP} , CA _{SIP} , CL _{SIP}	0.80	0.76	10.01	401.80
11	CW _{SIP} , MBA _{SIP} ** [*] , MBT _{SIP} , CWA _{SIP} [^] , FBH _{SIP} , H _{SIP} , DBH _{SIP} , MBL _{SIP} , CA _{SIP} , CL _{SIP} , AL _{SIP}	0.80	0.75	12.00	403.79

*p < 0.05; **p < 0.01; ***p < 0.001; [^]p < 0.1

oak trees as strictly monopodial; thus, defining the main axes of the oak trees with SIP was sometimes arbitrary. Nonetheless, more than 80% of the variance in H_{TLS} measurement was explained by H_{SIP}.

DBH was defined differently in case of both SIP and TLS methods. This could explain that DBH_{SIP} was constantly larger than DBH_{TLS}, which was not the case for tree height. Despite this, more than 90% of variance in DBH_{TLS} was explained by DBH_{SIP}. The result may be explained by the methodological assumptions of SIP, especially that the vertical plane of measurement cross sections target tree’s base, and the finding that the measurement error increases with distance to the plane of measurement (Gazda and Kędra 2017).

Table 7 Summary of the LMMs, created according to the formulas LMM[1a]-LMM[3d], and the reference linear models (LMs), to predict TLS-derived horizontal crown projection (CPA_{TLS}) with SIP-derived data, showing model prediction errors: RMSE1 (based on model fitted values), RMSE2 (based on a leave-one-out analysis); the best predictive model is denoted by italics; and all models’ coefficients are given in the [Electronic supplementary material](#)

Model ID	RMSE1 (m ²)	RMSE1 (%)	RMSE2 (m ²)	RMSE2 (%)
LM[1]	9.94	27.59	10.23	28.37
LMM[1a]	8.27	22.94	9.49	26.32
LMM[1b]	8.25	22.89	9.90	27.48
LM[2]	8.99	24.96	9.56	26.51
LMM[2a]	7.75	21.50	9.16	25.43
LMM[2b]	7.48	20.76	8.97	24.90
LMM[2c]	5.67	<i>15.75</i>	7.45	<i>20.66</i>
LM[3]	8.65	24.00	9.59	26.61
LMM[3a]	7.79	21.62	9.44	26.20
LMM[3b]	7.53	20.90	9.28	25.75
LMM[3c]	5.68	15.76	7.82	21.69
LMM[3d]	7.63	21.18	9.17	25.43

CPA area measured by TLS (CPA_{TLS}) was a 3D object-derived trait (Barbeito et al. 2017), and as such, it could not be measured with SIP. However, we found a close correlation between CPA_{TLS} and crown width (CW_{SIP}), which, supplemented with MBA_{SIP}, enabled effective modelling of CPA_{TLS}. The best predictive model LMM[2c] resulted on 15.8% RMSE1 and 20.7% RMSE2. We found RMSE2 more reliable, because it was based on a set of models’ errors, computed independently from the training data sets. The inclusion of the random (stand) effect improved predictions in all cases and was most effective when connected to branch angles. This confirms that branching angles are very sensitive to local environmental conditions such as tree density and species

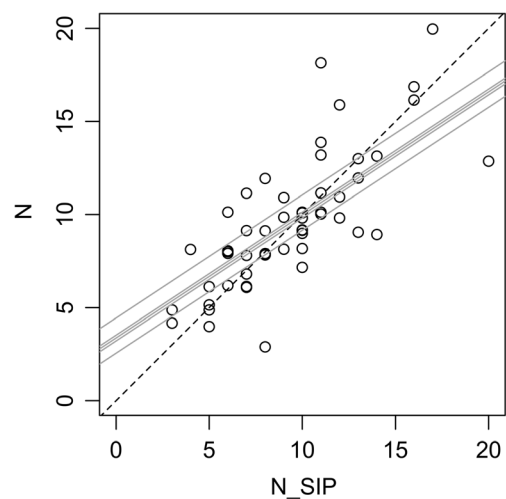


Fig. 5 Comparison of SIP (N_{SIP}) with field (N) tree counts within an 8-m distance from the target tree (for 54 plots); grey lines are the regression lines of a mixed effects model, where the random effect (on intercept) was stand with five levels: O214, O108, O255, O12, O57 and O598 (from largest to lowest intercept value); dashed line is the 45-degree line; the observations were jittered along the vertical axis to show overlapping points

Table 8 Mean values and standard deviations (SD) for the number of trees growing within 8 m from the target tree. N from field measurements and N_SIP estimated with SIP method; r = Pearson's correlation

Variable	Mean	SD	Correlation	
			r	p value
N	9.59	3.54	0.759	2.93E-11
N_SIP	9.35	3.56		

composition (Bayer et al. 2013). Branch length, on the contrary, seems to be more or less constant for a given diameter (Gazda and Kędra 2017). We suspect that this explains why DBH_{SIP} and AL_{SIP} were not included in the first five best subsets of variables to predict CPA_{TLS} .

4.2 Comparison with previous studies

Few studies have compared image-based with laser-based tree architectural traits measurements. One of such studies was done by Delagrangue and Rochon (2011) on an individual sapling (2 m high), analysed with TLS- and image-based data. It is difficult to directly compare that study with ours, because there was just one small tree sampled, and the photogrammetric method used multiple images and an algorithm to build a 3D (voxel) model ("TreeAnalyser"; Phattaralerphong and Sinoquet 2005), which preceded measurements. However, some of the analysed architectural traits were the same. For tree height, the image-based measurement attained the error of 4.5% (it was -0.5% for TLS); crown diameter (here as crown width) was overestimated from images by 9.7% (and 3.4% by TLS). In that context, the results for the SIP method were satisfactory. Results of that study confirm that comparison of a new method with TLS is a good calibration technique, the errors being always much lower in case of the laser-based measurements.

Bournez et al. (2017) compared their "TreeArchitecture" algorithm with two other methods for automated tree measurements from TLS data: "PlantScan3D" (Boudon et al. 2014) and "SimpleTree" (Hackenberg et al. 2015). They used six urban individual trees with different architectures; the reference measurements there were often connected to a manual, 3D tree skeletonization. For the number of detected branches, the error varied between -77.4 and 282.6%; for total length of branches, from -60.9 to 19.9%; and for DBH, from -37.5 to 4.9%. The CPA_{TLS} prediction error for an individual tree in our study ranged between -42 and 59%, which is a comparable range of errors, to those of that study. However, in TLS, when the automated work done by an algorithm is combined with manual corrections, the errors may be largely reduced (Momo Takoudjou et al. 2017).

Our comparison of crown projection area estimates with allometric models showed that all SIP-based models

performed much better in terms of the prediction error. Nonetheless, usefulness of such allometric models in many applications was confirmed, given the simplicity of that approach, and percentage RMSE below 50%. We found that the species-specific equation, created for *Q. robur*, gave better results than the general equation for the allometric type, which confirms that *Q. robur* and *Q. petraea* are very similar in terms of allometry (e.g. Forrester et al. 2017).

4.3 SIP method in forest monitoring and modelling

In recent years, many studies have focused on precise assessment of forest biomass (Forrester et al. 2017; Henry et al. 2011; Muukkonen 2007; Vallet et al. 2006). Some results suggest that tree crown variables may be very efficient in biomass models since crown dimensions are sensitive to many stand structural characteristics and can therefore potentially replace stand variables in biomass equations (Forrester et al. 2017). However, direct crown measurements are time consuming and thus rarely available. Therefore, stem diameter is still the most commonly used variable for aboveground biomass estimations. Our results are congruous with existing studies; DBH_{SIP} in our analysis of best predictors for CPA_{TLS} , appeared for the first time only in the sixth subset (Table 6). Large-scale collection of the tree architectural traits may be potentially facilitated by SIP method, which represents an alternative to derive such variables. This paper shows that the data obtained from SIP may be consistent with the state-of-the-art TLS method. Moreover, it may also provide a coarse measure of local competition, in terms of number of neighbours (Sect. 3.4). As such, SIP could be included in forest monitoring projects, when the sampling is at an individual tree level, especially when TLS is unlikely to be used. Yet, SIP and TLS methods may also be combined, for further validation of SIP, but also because the information gained differs: a photograph still remains an easily recognized, archived and comparable medium.

4.4 Limitations of SIP method and practical recommendations

The presence of evergreen trees may reduce SIP accuracy or precision, as shown for tree height and crown width measurements (Table 5). However, whether these reductions were caused by increased occlusion, differences in the architecture of target trees in mixed neighbourhood, or both, remain unclear. Larger crowns may cause larger occlusion of tree tops (in the photograph, part of the crown edge may appear as the highest point of a tree), resulting in an overestimation of tree height. This could explain the increased deviation and the positive bias of H_{SIP} measurement in mixed stands, as we expected larger crowns under mixed species composition (Barbeito et al. 2017). The drop in precision of CW_{SIP} is most

probably connected to noisier background in the presence of pines and considerable difficulties in visual tracing of thin branches forming the crown edge. Most likely, this problem would grow with increasing share of conifers. Higher stand density may cause reduced light conditions (poor quality photographs), and noisier background; however, given the range of tree density in our study, crown measurements were not significantly affected by the factor.

SIP is, at most times, easily applied to solitary trees; on the contrary, it is not possible to measure large canopy trees with SIP method in a dense deciduous forest with overlapping crowns, in the leaf-on season. Between those two extremes, there is a huge space for SIP applications. Here, we tested the method in a lowland, managed-type forest. Previously, the method was successfully applied in an upland, natural European beech (*Fagus sylvatica* L.) forest, with some admixture of conifers (Gazda and Kędra 2017), in both cases in the leafless season. This condition must be fulfilled, if branching of deciduous trees is to be assessed. When choosing the time for SIP measurement, it is necessary to consider that in late winter/early spring the days are longer, and thus light conditions may be better than in late fall/early winter. The presence of ground snow may be a helping factor, by providing a clear and contrasted background of tree stems (own observation). We recommend a previous visit to the trees of interest when SIP is planned to be used to check if the trees can be captured with a single image and visually distinguished from the background.

5 Conclusion

Our results provide evidence that SIP can be successfully applied to obtain accurate tree architectural traits in mature forests. Since the correlation with TLS is high, SIP could be used as an alternative method to obtain tree architecture when terrain limits the use of TLS such as in heterogeneous mountain landscapes. As inferred from Delagrange and Rochon (2011), yielding an image-based 3D point cloud could be not a feasible solution, when it is mostly useful for measuring so-called 2D traits. Consequently, we showed that a simplified photogrammetric method, allowing to skip the steps leading to a virtual 3D model, may bring reliable tree architecture measurements. We presented a choice of linear and linear mixed effects CPA models from SIP variables. Our comparison was tested in a single site but with a large variation in tree crown sizes and shapes, and a range of tree densities representative of many temperate forests. However, future research could focus on further validation of the models presented and transferability of our results to other situations with tree species differing in their architectural properties (like branching pattern), size, age and growing conditions.

Acknowledgements Vast majority of the SIP data were extracted during a 4-week stay of K.K. at the INRA LERFoB office in Champenoux, France, within a hosting agreement between INRA and University of Agriculture in Krakow, under the supervision of I.B. We acknowledge the kind assistance of Camille Couteau and Vincent Seigner during data collection in the OPTMix experimental site, Orléans National Forest.

Funding K.K. was funded by the COST (European Cooperation in Science and Technology) Action FP1206 EuMIXFOR (COST-STSM-ECOST-STSM-FP1206-150316-071762). I.B. was funded by the French National Research Agency through the Laboratory of Excellence ARBRE (ANR-12-LABXARBRE-01), in particular through the Scan-Comp project. The OPTMix site belongs to the SOERE F-ORET which is supported annually by Ecofor, Allenvi, and the French National Research Infrastructure, ANAEE-F (<http://www.anaee-france.fr/fr/>). The study was also supported by the Polish Ministry of Science and Higher Education grant no. DS 3421/ZBL.

Data availability The data that support the findings of this study are available from Irstea (OPTMix database) but restrictions apply to the availability of these data, which were used under licence for the current study, and so are not publicly available. Data are however available from the authors upon reasonable request and with permission of Irstea.

Compliance with ethical standards

Conflict of interest The authors declare that they have no conflict of interest.

Open Access This article is distributed under the terms of the Creative Commons Attribution 4.0 International License (<http://creativecommons.org/licenses/by/4.0/>), which permits unrestricted use, distribution, and reproduction in any medium, provided you give appropriate credit to the original author(s) and the source, provide a link to the Creative Commons license, and indicate if changes were made.

Publisher's note Springer Nature remains neutral with regard to jurisdictional claims in published maps and institutional affiliations.

References

- Barbeito I, Collet C, Ningre F (2014) Crown responses to neighbor density and species identity in a young mixed deciduous stand. *Trees* 28:1751–1765. <https://doi.org/10.1007/s00468-014-1082-2>
- Barbeito I, Dassot M, Bayer D, Collet C, Drossler L, Lof M, del Rio M, Ruiz-Peinado R, Forrester DI, Bravo-Oviedo A, Pretzsch H (2017) Terrestrial laser scanning reveals differences in crown structure of *Fagus sylvatica* in mixed vs. pure European forests. *For Ecol Manag* 405:381–390. <https://doi.org/10.1016/j.foreco.2017.09.043>
- Barthélémy D, Caraglio Y (2007) Plant architecture: a dynamic, multi-level and comprehensive approach to plant form, structure and ontogeny. *Ann Bot* 99:375–407. <https://doi.org/10.1093/aob/mcl260>
- Bates D, Machler M, Bolker BM, Walker SC (2015) Fitting linear mixed-effects models using lme4. *J Stat Softw* 67:1–48
- Bayer D, Seifert S, Pretzsch H (2013) Structural crown properties of Norway spruce (*Picea abies* L. Karst.) and European beech (*Fagus sylvatica* L.) in mixed versus pure stands revealed by terrestrial laser scanning. *Trees* 27:1035–1047. <https://doi.org/10.1007/s00468-013-0854-4>
- Boudon F, Preuksakam C, Ferraro P, Diener J, Nacry P, Nikinmaa E, Godin C (2014) Quantitative assessment of automatic reconstructions of branching systems obtained from laser scanning. *Ann Bot* 114:853–862. <https://doi.org/10.1093/aob/mcu062>

- Boumez E, Landes T, Saudreau M, Kastendeuch P, Najjar G (2017) From TLS point clouds to 3D models of trees: a comparison of existing algorithms for 3D tree reconstruction. *Int Arch Photogramm Remote Sens Spatial Inf Sci*, Vol XLII-2/W3: Proceedings of the 7th Workshop on 3D Virtual Reconstruction and Visualization of Complex Architectures XLII-2/W3:113–120. <https://doi.org/10.5194/isprs-archives-Q7XLII-2-W3-113-2017>
- Calders K, Newnham G, Burt A, Murphy S, Raunonen P, Herold M, Culvenor D, Avitabile V, Disney M, Armston J, Kaasalainen M (2015) Nondestructive estimates of above-ground biomass using terrestrial laser scanning. *Methods Ecol Evol* 6:198–208. <https://doi.org/10.1111/2041-210X.12301>
- Dassot M, Colin A, Santenoise P, Fournier M, Constant T (2012) Terrestrial laser scanning for measuring the solid wood volume, including branches, of adult standing trees in the forest environment. *Comput Electron Agric* 89:86–93. <https://doi.org/10.1016/j.compag.2012.08.005>
- Delagrangé S, Rochon P (2011) Reconstruction and analysis of a deciduous sapling using digital photographs or terrestrial-LiDAR technology. *Ann Bot* 108:991–1000. <https://doi.org/10.1093/aob/mcr064>
- Durand Y, Brun E, Merindol L, Guyomarch G, Lesaffre B, Martin E (1993) A meteorological estimation of relevant parameters for snow models. *Ann Glaciol*, Vol 18: Proceedings of the Symposium on Snow and Snow-Related Problems 18: 65–71. <https://doi.org/10.1017/s0260305500011277>
- Eaton E, Caudullo G, Oliveira S, de Rigo D (2016) *Quercus robur* and *Quercus petraea* in Europe: distribution, habitat, usage and threats. In: San-Miguel-Ayán J, de Rigo D, Caudullo G, Houston Durrant T, Mauri A (eds) *European atlas of forest tree species*. Publ. Off. EU, Luxembourg, pp 160–163
- Fleck S, Moelder I, Jacob M, Gebauer T, Jungkunst HF, Leuschner C (2011) Comparison of conventional eight-point crown projections with LIDAR-based virtual crown projections in a temperate old-growth forest. *Ann For Sci* 68:1173–1185. <https://doi.org/10.1007/s13595-011-0067-1>
- Forrester DI, Tachauer IHH, Annighoefer P, Barbeito I, Pretzsch H, Ruiz-Peinado R, Stark H, Vacchiano G, Zlatanov T, Chakraborty T, Saha S, Sileshi GW (2017) Generalized biomass and leaf area allometric equations for European tree species incorporating stand structure, tree age and climate. *For Ecol Manag* 396:160–175. <https://doi.org/10.1016/j.foreco.2017.04.011>
- Gazda A, Kędra K (2017) Tree architecture description using a single-image photogrammetric method. *Dendrobiology* 78:124–135. <https://doi.org/10.12657/denbio.078.012>
- Hackenberg J, Spiecker H, Calders K, Disney M, Raunonen P (2015) SimpleTree—an efficient open source tool to build tree models from TLS clouds. *Forests* 6:4245–4294. <https://doi.org/10.3390/f6114245>
- Hebbali A (2017) ‘olsrr’ v.0.4.0 R package: tools for building OLS regression models
- Henry M, Picard N, Trotta C, Manlay RJ, Valentini R, Bernoux M, Saint-Andre L (2011) Estimating tree biomass of sub-Saharan African forests: a review of available allometric equations. *Silva Fenn* 45: 477–569. <https://doi.org/10.14214/sf.38>
- IUSS Working Group (2014) World reference base for soil resources. 2014, Vol. 106: world soil resources reports. International soil classification system for naming soils and creating legends for soil maps (ed) FAO, Rome
- Korboulewsky N, Pérot T, Balandier P, Ballon P, Barrier R, Boscardin Y, Dauffy-Richard E, Dumas Y, Ginisty C, Gosselin M, Hamard J-P, Laurent L, Mârell A, NDiaye A, Perret S, Rocquencourt A, Seigneur V, Vallet P (2015) OPTMix—Dispositif expérimental de suivi à long terme du fonctionnement de la forêt mélangée. *Rendez-Vous Techniques de l’ONF* 47:60–70
- Lee CA, Voelker S, Holdo RM, Muzika RM (2014) Tree architecture as a predictor of growth and mortality after an episode of red oak decline in the Ozark Highlands of Missouri, U.S.A. *Can J For Res* 44:1005–1012. <https://doi.org/10.1139/cjfr-2014-0067>
- Legendre P (2014) lmodel2: Model II Regression. R package version 1.7-2
- Liang XL, Kankare V, Hyypä J, Wang YS, Kukko A, Haggren H, Yu XW, Kaartinen H, Jaakkola A, Guan FY, Holopainen M, Vastaranta M (2016) Terrestrial laser scanning in forest inventories. *ISPRS J Photogramm Remote Sens* 115:63–77. <https://doi.org/10.1016/j.isprsjprs.2016.01.006>
- Martin-Ducup O, Schneider R, Fournier RA (2016) Response of sugar maple (*Acer saccharum*, Marsh.) tree crown structure to competition in pure versus mixed stands. *For Ecol Manag* 374:20–32. <https://doi.org/10.1016/j.foreco.2016.04.047>
- Momo Takoudjou S, Ploton P, Sonké B, Hackenberg J, Griffon S, Rouault De Coligny F, Kamdem NG, Libalah M, Mofack GI, Le Moguedec G, Pelissier R, Barbier N (2017) Using terrestrial laser scanning data to estimate large tropical trees biomass and calibrate allometric models: a comparison with traditional destructive approach. *Methods Ecol Evol* 9:905–916. <https://doi.org/10.1111/2041-210X.12933>
- Muukkonen P (2007) Generalized allometric volume and biomass equations for some tree species in Europe. *Eur J For Res* 126:157–166. <https://doi.org/10.1007/s10342-007-0168-4>
- Oldeman RAA (1990) *Forests: elements of silvology*. Springer-Verlag, Berlin
- Phattaralerphong J, Sinoquet H (2005) A method for 3D reconstruction of tree crown volume from photographs: assessment with 3D-digitized plants. *Tree Physiol* 25:1229–1242
- Poorter L, Bongers F, Sterck FJ, Woll H (2003) Architecture of 53 rain forest tree species differing in adult stature and shade tolerance. *Ecology* 84:602–608. [https://doi.org/10.1890/0012-9658\(2003\)084\[0602:aorfts\]2.0.co;2](https://doi.org/10.1890/0012-9658(2003)084[0602:aorfts]2.0.co;2)
- Poorter L, Bongers L, Bongers F (2006) Architecture of 54 moist-forest tree species: traits, trade-offs, and functional groups. *Ecology* 87: 1289–1301. [https://doi.org/10.1890/0012-9658\(2006\)87\[1289:aomstj\]2.0.co;2](https://doi.org/10.1890/0012-9658(2006)87[1289:aomstj]2.0.co;2)
- Pretzsch H, Biber P, Uhl E, Dahlhausen J, Rotzer T, Caldentey J, Koike T, van Con T, Chavanne A, Seifert T, du Toit B, Farnden C, Pauleit S (2015) Crown size and growing space requirement of common tree species in urban centres, parks, and forests. *Urban For Urban Green* 14:466–479. <https://doi.org/10.1016/j.ufug.2015.04.006>
- Pya N, Voinov V, Makarov R, Voinov Y (2016) mvnTest: goodness of fit tests for multivariate normality. R package version 1.1-0
- QGIS Development Team (2016) QGIS geographic information system. Open Source Geospatial Foundation Project
- R Core Team (2017) R: a language and environment for statistical computing. R Foundation for Statistical Computing, Vienna
- Rust S, Roloff A (2002) Reduced photosynthesis in old oak (*Quercus robur*): the impact of crown and hydraulic architecture. *Tree Physiol* 22:597–601
- Saenz-Romero C, Lamy JB, Ducouso A, Musch B, Ehrenmann F, Delzon S, Cavers S, Chalupka W, Dagdas S, Hansen JK, Lee SJ, Liesebach M, Rau HM, Psomas A, Schneck V, Steiner W, Zimmermann NE, Kremer A (2017) Adaptive and plastic responses of *Quercus petraea* populations to climate across Europe. *Glob Chang Biol* 23:2831–2847. <https://doi.org/10.1111/gcb.13576>
- Takahashi K (1996) Plastic response of crown architecture to crowding in understory trees of two co-dominating conifers. *Ann Bot* 77:159–164. <https://doi.org/10.1006/anbo.1996.0018>
- Vallet P, Dhote JF, Le Moguedec G, Ravart M, Pignard G (2006) Development of total aboveground volume equations for seven important forest tree species in France. *For Ecol Manag* 229:98–110. <https://doi.org/10.1016/j.foreco.2006.03.013>
- Van de Peer T, Verheyen K, Kint V, Van Cleemput E, Muys B (2017) Plasticity of tree architecture through interspecific and intraspecific competition in a young experimental plantation. *For Ecol Manag* 385:1–9. <https://doi.org/10.1016/j.foreco.2016.11.015>